measured absolute values of H_{ct} and H_{c4} very meaningful.

In conclusion, we would like to note that we certainly do not believe we have proved experimentally the existence of something like H_{c4} unambiguously. Most of our experiments can be explained by assuming inhomogeneous parts in the bulk of the films. However we think we have shown that wedge-shaped geometries behave differently from film geometries in magnetic fields, and it may even be that inhomogeneous parts can be considered as wedge shaped, which would correspond to an H_{c4} model.

Part of this work has been supported by the Foundation for Fundamental Research on Matter (Stichting voor Fundamenteel Onderzoek der Materie) with financial support from the Nederlandse Organisake voor Zwiver-Wetenschappelijk Onderzoek (Z. W. O.).

[1]For a recent review see, e.g., W. C. H. Joiner, Phil. Mag. 20, 807 (1969).

[2]D. Saint-James and P. G. de Gennes, Phys. Letters 7, 306 (1963).

[3]A. Houghton and F. B. McLean, Phys. Letters 19, 172 (1965).

[4]A. P. van Gelder, Phys. Rev. Letters 20, 1435 (1968).

[5]H. J. Fink, Phys. Rev. 177, 1017 (1969).

[6]V. L. Ginzburg and L. D. Landau, Zh. Eksperim. i Teor. Fiz. 20, 1064 (1950).

[7]For a preliminary report on these investigations see A. P. van Gelder, J. W. Hendriks, and P. Wyder, in *Proceedings of the Eleventh International Conference on Low Temperature Physics, St. Andrews*, 1968, edited by J. F. Allen, D. M. Finlayson, and D. M. McCall (St. Andrew's U. P., St. Andrew's, Scotland, 1969), Vol. II, p. 956.

[8]P. G. de Gennes, *Superconductivity of Metals and Alloys* (Benjamin, New York, 1966).

[9]H. N. de Lang, Doctoraalscriptie, University of Nijmegen, The Netherlands, 1969 (unpublished).

[10]See, e.g., V. L. Newhouse, *Applied Superconductivity* (Wiley, New York, 1964).

[11]M. Tinkham, Phys. Rev. 129, 2413 (1963).

[12]F. E. Harper and M. Tinkham, Phys. Rev. 172, 441 (1968).

PHYSICAL REVIEW B VOLUME 4, NUMBER 9 1 NOVEMBER 1971

Neutron Scattering Study of the Lattice-Dynamical Phase Transition in Nb_3Sn†

G. Shirane and J. D. Axe
Brookhaven National Laboratory, Upton, New York 11973

(Received 17 May 1971)

Neutron scattering experiments have been carried out on a single crystal of Nb_3Sn through the lattice-dynamical phase transition at $T_m = 45$ °K. A small tetragonal lattice distortion, $a/c = 1.0062$ at 4 °K, was previously established by x-ray studies, but sublattice displacements below T_m have remained undetermined. The present study reveals that the tetragonal phase exhibits *new* Bragg reflections, which are forbidden by symmetry in the cubic phase. From the intensity distribution among these new reflections, the structure was determined uniquely as D^9_{4h} with Nb displacements from the special positions of 0.016(3) Å at 4 °K. Only the Nb sublattices shift, and in a pattern identical with the eigenvectors of the $\Gamma_{12}(+)$ $q = 0$ optic-phonon mode in the cubic phase. Such a mode is *linearly* coupled with the soft [110] shear acoustic mode. This linear coupling requires, and our measurements confirm, that the intensities of new Bragg peaks are proportional to $(a/c - 1)^2$. An optic-phonon instability is *not* required to explain these internal displacements.

I. INTRODUCTION

In recent years, extensive investigation has been carried out on many lattice-dynamical phase transitions. One of the most fascinating phase transitions known of this type occurs in high-temperature superconductors with the β-W structure (type A-15).[1] This phase transition takes place, on cooling, before the onset of the superconducting state. It is accompanied by a remarkable elastic softening, in particular, for shear modes with wave vector $\vec{q} \parallel [110]$ and polarization vector $\vec{e} \parallel [1\bar{1}0]$. For example, in the case of Nb_3Sn, the acoustic velocity[2] falls from a normal room-temperature value to near zero around $T_m = 45$ °K. The crystal is cubic above T_m and becomes tetragonal[3] below T_m with $a/c = 1.0062$ at 4 °K.

Many experimental and theoretical studies have been published[4] on this phase transition in Nb_3Sn, as well as on the similar transition in V_3Si at 21 °K. There are, nevertheless, fundamental questions concerning the nature of the transformation which remain unsolved. Anderson and Blount[5] pointed out that if the phase change is truly of second order the tetragonal strain cannot be the primary-order parameter, and they raised the pos-

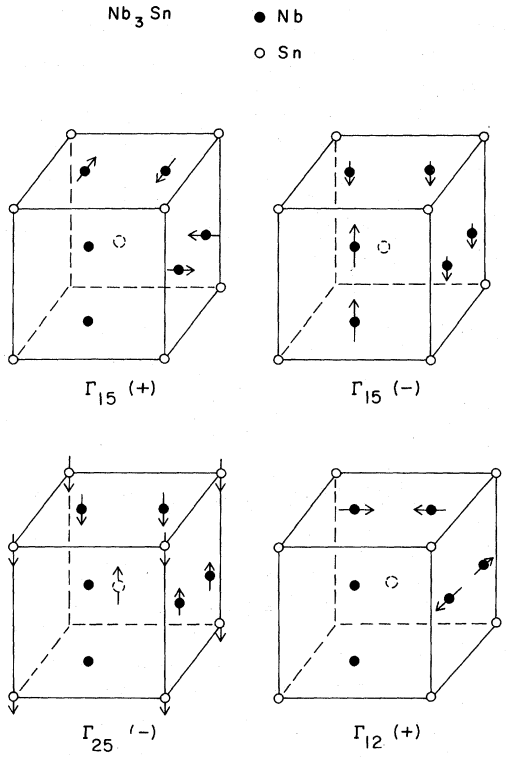

FIG. 1. Four models of Nb_3Sn atomic shifts discussed by Perel, Batterman, and Blount (Ref. 6).

sibility of the instability and resultant condensation of an optic-phonon mode, which produce an elastic strain through higher-order coupling. Subsequently, Perel, Batterman, and Blount[6] reported a careful search for sublattice distortions in V_3Si which would result from such a mechanism. They attempted, and failed, to detect x-ray reflections from the "forbidden" (221)-type reflections in the low-temperature tetragonal phase. Their paper presented a careful and detailed discussion of expected atomic shifts based on the group-theoretical arguments. Brillouin-zone-center optic-phonon eigenvectors of four symmetry types are compatible with a tetragonal low-temperature structure. They belong to the representations $\Gamma_{25}(-)$, $\Gamma_{15}(-)$, $\Gamma_{15}(+)$, and $\Gamma_{12}(+)$, and are shown in Fig. 1 and Table I. Recently, Klein and Birman[7] presented theoretical calculations which showed how in some instances the $\Gamma_{25}(-)$ and $\Gamma_{15}(-)$ mode frequencies could soften by "overscreening" from the *d* electrons. On the other hand, the various elaborations of the Labbé-Friedel model[8–10] invoke only direct electron–acoustic-phonon coupling and thus a (first-order) instability involving only acoustic-phonon modes.

The present experiments establish the presence in Nb_3Sn of sublattice displacements of the $\Gamma_{12}(+)$ type. Because these sublattice displacements can be driven by a linear piezo-optic coupling to the tetragonal strain, no optic-phonon instability is required to explain these observations.

TABLE I. Relative atomic positions in the cubic tetragonal Nb_3Sn for different representations, following the format adopted by Perel, Batterman, and Blount (Ref. 6).

	O_h^3 Cubic	C_{4v}^7 $\Gamma_{15}(-)$	D_{2d}^5 $\Gamma_{25}(-)$	C_{4h}^2 $\Gamma_{15}(+)$	D_{4h}^9 $\Gamma_{12}(+)$
Nb	$\frac{1}{2}\ 0\ \frac{1}{4}$	$0, 0, 2\delta$			
	$\frac{1}{2}\ 0\ \frac{3}{4}$	2δ			
	$0\ \frac{1}{4}\ \frac{1}{2}$	$-\delta$	$0, 0, \delta$	$\delta, 0, 0$	$0, -\delta, 0$
	$0\ \frac{3}{4}\ \frac{1}{2}$	$-\delta$	δ	$-\delta$	δ
	$\frac{1}{4}\ \frac{1}{2}\ 0$	$-\delta$	$-\delta$	δ	δ
	$\frac{3}{4}\ \frac{1}{2}\ 0$	$-\delta$	$-\delta$	$-\delta$	$-\delta$
Sn	$0\ 0\ 0$	s	$-s$		
	$\frac{1}{2}\ \frac{1}{2}\ \frac{1}{2}$	s	$+s$		

II. SCATTERING EXPERIMENT

Neutron diffraction data were collected at the Brookhaven High Flux Beam Reactor on a single crystal of Nb_3Sn made available to us by Batterman. The crystal was grown by Hanak and Berman[11] and was used in a previous x-ray investigation.[3] The volume, 0.05 cm^3, is large for elastic diffraction studies but quite small for inelastic scattering. Our experiments place the transformation temperature $T_m = (45.2 \pm 0.3)$ °K about 2 °K higher than the value reported in the x-ray study of the same crystal.[3] More recent x-ray studies[12] have indicated $T_m = 44$ and 51 °K for two crystals examined. It appears that the transition is sensitive to internal strains and may thus not be uniform within a given crystal.

A. Symmetry of the Tetragonal Phase

Preliminary estimates of the intensity distribution to be expected from low index reflections which are forbidden in the cubic ($Pm3n$ or O_h^3) phase are shown in Table II for displacements of the four possible symmetry types. We have arbitrarily assumed values for Nb sublattice displacements δ of $0.002a$–$0.003a$. For comparison the strengths of some allowed reflections are also calculated. Even in making reliable *qualitative* observations of such very weak "forbidden" reflections extraordinary care must be taken to eliminate two sources of spurious reflections.

(i) The incident beam must be free from $\lambda/2$ contamination. We therefore selected relatively low incident neutron energies (13.5–15.5 meV or 2.5–2.7 Å) to take advantage of recently developed high-efficiency pyrolytic graphite filters[13] for $\lambda/2$ elimination. A 4-in. filter thickness reduces $\lambda/2$

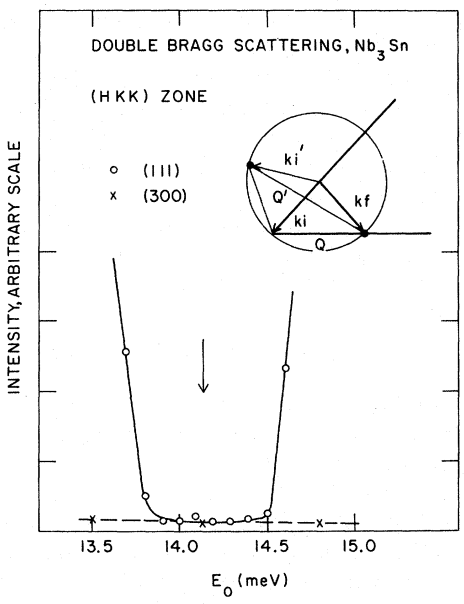

FIG. 2. Study of double Bragg contamination by changing neutron energy E_0. The (300) is clean, while the (111) is heavily contaminated at both ends.

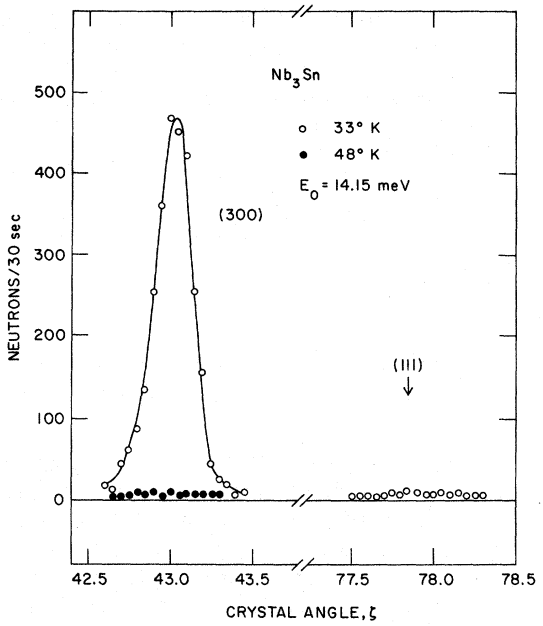

FIG. 3. Intensities of "new" reflections in Nb_3Sn, which are forbidden in the cubic phase.

by a factor 10^5–10^6 with a loss of only 50% primary intensity.

(ii) Double Bragg scattering. This arises (see Fig. 2) when the sphere of reflection accidentally passes through two reciprocal-lattice points, and occurs rather frequenctly in neutron diffraction because of the relatively nonmonochromatic nature of the incident beam. The use of a low incident energy, tight collimation, and the narrow crystal mosaic (< 6 min in the cubic phase) all help to decrease the double scattering probability. On the other hand, the tetragonal distortion and twinning below T_m increase the probability of double scattering.

The conventional technique for checking for the presence of double Bragg scattering is to rotate the crystal about the scattering vector. This is rather tedious and sometimes not entirely conclusive. In neutron scattering one has the alternative possibility of continuously varying the incident

TABLE II. Calculated intensities $I = F^2/\sin 2\theta$, with F^2 in units of 10^{-4} b per unit cell, and $\sin 2\theta$ for 14.8-meV neutrons. The Sn shift s in Table I was assumed to be zero. $b_{Nb} = 0.71$, $b_{Sn} = 0.61 \times 10^{-12}$ cm.

$10^3\delta$	0	2	3	3	3	−3
Mode	Cubic	$\Gamma_{15}(-)$	$\Gamma_{25}(-)$	$\Gamma_{15}(+)$	$\Gamma_{12}(+)$	$\Gamma_{12}(+)$
(111)	0	0	0	40	0	0
(300)	0	0	0	0	65	65
(003)	0	0	260	0	0	0
(110)	680	680	680	680	370	1100
(101)	680	690	690	680	880	510
(200)	87 700	87 700	87 700	87 600	87 800	87 800
(002)	87 700	88 000	87 600	87 400	87 400	87 400

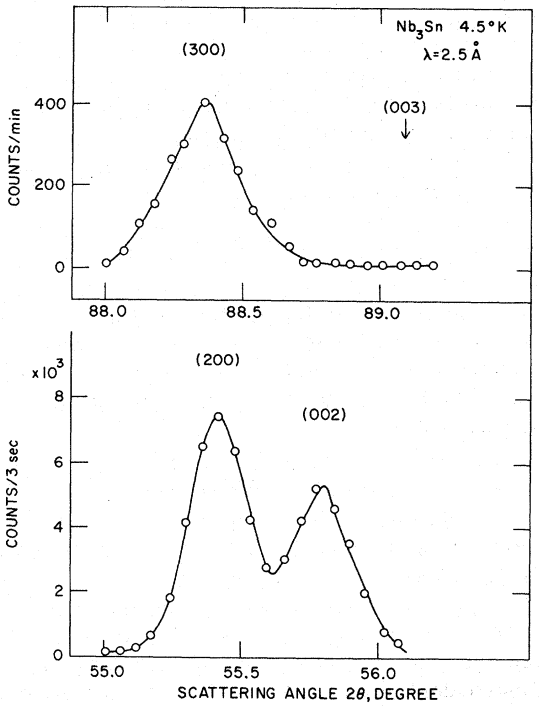

FIG. 4. Domain distribution in the tetragonal phase of Nb_3Sn. These data were taken with tight collimation as described in the text.

TABLE III. Observed structure factors $F_{obs}^2 = I\sin 2\theta$ of new reflections in Nb_3Sn at 33 °K. Data are composites of several scans using 13.5-, 14.1-, 14.8-, and 15.4-meV neutrons as explained in the text, with ±20% in estimated errors. Temperature factor is small enough to be neglected in this range.

hkl	F_{calc}, $\Gamma_{12}(+)$	F_{obs}^2
300	180	190
100	20	23
111	0	<2
311	320	310
122	20	17

neutron energy (and thus changing the radius of the sphere of reflection). Figure 2 shows examples of two such energy scans in the (*HKK*) zone taken at 48 °K. The (300) reflection is quite clean over the whole energy range while the (111) reflection is contaminated at both ends of the spectrum. By selecting the center of the clean region, 14.15 meV, one is guaranteed to be free from double Bragg effect even if the tetragonal distortion slightly broadens the contaminated region.

There is one very special case of double Bragg scattering which is unaffected by a change of incident energy. This arises if a reciprocal-lattice point exists on the circular intersection between the sphere of reflection and a plane perpendicular to the scattering plane but containing $\vec{Q}$. This intersection remains the same when we change energy. One can accurately predict this occurrence in a given scattering plane and remove it by rotating the crystal around the scattering vector. As we shall see later, it is quite important to know that the (111) reflection is missing in the tetragonal phase, as shown in Fig. 3.

Energy scans, such as shown in Fig. 2, were carried out at 48 °K on many reflections of the types shown in Table II. Forbidden reflections were often found to be strongly contaminated; thus it required four different neutron energies: 13.5, 14.15, 14.8, and 15.4 meV, to collect a complete set of reliable intensity data for the forbidden reflections.

It must be noted that the double Bragg contamination increases rapidly with the energy of radiation. Our preliminary results at $E_0 = 80$ meV ($\lambda = 1$ Å) indicated that the use of low-energy neutrons has a great advantage for this type of study.

Examples of data taken with due regard to the above considerations are shown in Fig. 3. The appearance and growth of "forbidden" peaks in the tetragonal phase are clearly observed although they have < 0.1% of the strength of strong fundamentals. Inspection of Table II reveals that the existence of a "forbidden" (300) reflection eliminates all but $\Gamma_{25}(-)$ and $\Gamma_{12}(+)$ type displacements. If we could distinguish between $(300)_t$ and $(003)_t$ an unambigous assignment would be possible. By tightening the beam collimation (10 min before and after the sample) and inserting an analyzing crystal (pyrolytic graphite) to further increase the resolution, it was possible to establish from a careful survey that $(003)_t$ is entirely missing (see Fig. 4). We therefore conclude that sublattice displacements of symmetry type $\Gamma_{12}(+)$ are present in the tetragonal structure.

B. Magnitude of the Sublattice Displacements

While in favorable cases the individual domain contributions can be resolved, the tight collimation is not ideal for quantitative comparison of intensities. Therefore, in order to study the magnitude of the $\Gamma_{12}(+)$ distortion, which involves the comparison of forbidden reflections with standard allowed ones, we chose the conventional two-axis configuration with relaxed collimation after the sample allowing the instrument to integrate over the domain distribution.

As we have just discussed, in the tetragonal phase the intensity of Bragg scattering from the region in reciprocal space denoted as (*HKL*) in the cubic phase is given by $\alpha I(HKL)_t + \beta I(LHK)_t + \gamma I(KLH)_t$, the fractions α, β, γ depending upon the domain distribution in the sample. It is im-

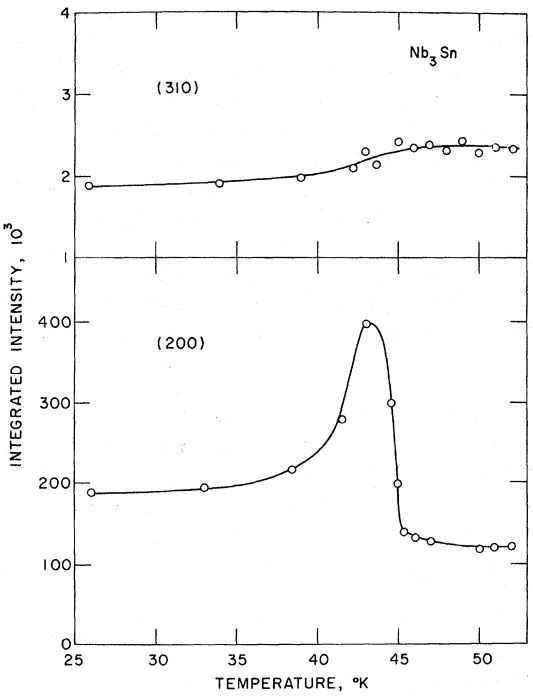

FIG. 5. Study of extinction effect through the phase transition. The strong (200) reflection shows a peak due to a domain formation.

TABLE IV. Crystallographic data of Nb_3Sn at 4 °K. Lattice constants are taken from Ref. 3. The origin of this table is shifted by $(\frac{1}{2},0,0)$ from the one in Table I. Forbidden reflections hhl: $l=2n+1$.

$a=5.293$ Å	$a/c=1.0062$
$x=\frac{1}{4}-\delta$	$\lvert\delta\rvert=0.0031(5)$
Space group $D_{4h}^9-P4_2/mmc$	
2 Sn at $2d$ $0,\frac{1}{2},\frac{1}{2}$	$\frac{1}{2},0,0$
2 Nb at $2l$ $0,0,\frac{1}{4}$	$0,0,\frac{3}{4}$
4 Nb at 4m $x,\frac{1}{2},0$	$\bar{x},\frac{1}{2},0$
$\frac{1}{2},x,\frac{1}{2}$	$\frac{1}{2},\bar{x},\frac{1}{2}$

possible, in general, to make a meaningful comparison of relative intensities of two (composite) reflections, unless α, β, and γ are known. Fortunately for the forbidden reflections in the (HKK) zone $I(K,\ K,\ H=\text{odd})_t=0$ and the composite twin intensity becomes $(\alpha+\beta)I(HKK)_t$, so that these reflections can be intercompared independent of the (unknown) domain distribution. This comparison is made in Table III.

On the other hand, the scaling of forbidden and standard reflection is affected by domain distribution. We chose to do this scaling in the $(HK0)$ zone using the average value $\frac{1}{2}[I(300)+I(030)]=kI(300)_t$. One can show that $\frac{1}{2}<k<1$. This weighting factor k was determined by the observed splittings of (200) and (020) peaks, as shown in Fig. 4.

The remaining problem which has bearing on the determining $|\delta|$ is extinction. Fortunately, there are groups of allowed reflections [both types $(4n,$ odd, odd) and $(4n,\ 4n+2,\ 4n+2)$] which are extremely weak, and thus likely to be free from extinction effects. We have verified this expectation by investigating the temperature dependence of intensities of the (310) and (200) reflections. Figure 5 shows a strong peaking in the (200) intensity just below T_m; this is due to a reduced extinction effect by a domain formation. On the other hand, the (310) reflection, which is 10^2 times weaker than (200), does not reveal any such extinction effect.

Final integrated intensities were collected by using four different energies: 13.5, 14.15, 14.8, and 15.4 meV and at temperatures 33, 38, and 48 °K. These high temperatures, rather than 4 °K, were selected to minimize the adverse effect of tetragonal distortion on the integrated intensities. The results summarized in Table III serve to completely confirm our choice of the $\Gamma_{12}(+)$ distortion. Table IV and Fig. 6 describe the tetragonal structure and atomic positions in the conventional low-temperature space group D_{4h}^9. The Nb shift $|\delta|$ was determined at 4.5 °K to be

$$|\delta|=0.0031(5)\ .$$

The sign of δ remains undetermined, although steric consideration would seem to strongly favor $\delta>0$ since $a>c$ (see Fig. 6). The sign of δ can in principle be determined from the intensity of (110)-type reflections (see Table II) but domain averaging reduces the expected difference to below the point of reliable detection.

Finally, we have examined the temperature dependence of the sublattice distortion by studying the temperature variation of the (300) reflection. The results are shown in Fig. 7. The solid line in Fig. 7, to which our data are normalized, is the square of the tetragonal strain $(a/c-1)^2$, taken from recent x-ray measurements.[9] Since the forbidden Bragg intensity is proportional to $|\delta|^2$, this establishes that *the internal sublattice displacements are proportional to the spontaneous tetragonal strain.*

We were not, however, able to observe a sharp discontinuity in the (300) intensity at the transformation. Since, on theoretical grounds (see Sec. II), we believe the transformation to be of first order, it is possible that the expected discontinuity is smeared out by an inhomogeneous T_m. That the behavior of Nb_3Sn near T_m is quite sample dependent has already been established.

III. DISCUSSION

Having established the existence of sublattice displacements in tetragonal Nb_3Sn, we must now understand their significance, particularly with respect to the Anderson-Blount proposal that such distortions may constitute the true order parameter for such transformations.[5] The essential feature of their idea is contained in a free energy expansion of the form

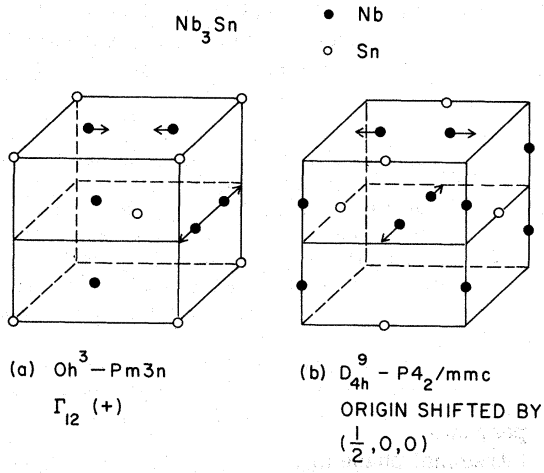

FIG. 6. $\Gamma_{12}(+)$ mode compared with the crystallographic description on the right-hand side, which exhibits tetragonal features more clearly.

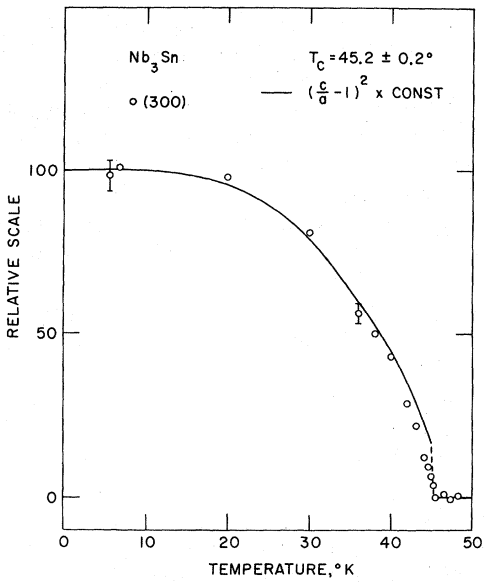

FIG. 7. Temperature dependence of (300) reflection. Solid line corresponds to the spontaneous tetragonal strain. Strictly speaking, the abscissa is $\alpha(T/T_m)$ with $\alpha = 45.2$. This was done to compensate for the variation in T_m between the samples compared.

$$F_0 = (\tfrac{1}{2}\omega_0^2 Q_0^2 + \tfrac{1}{4} V_4 Q_0^4 + \cdots) + \tfrac{1}{2} cu^2 + dQ_0^2 + \cdots , \quad (1)$$

where Q_0 represents the amplitude of a Brillouin-zone-center optical-phonon mode which "freezes" into the lattice at the temperature, T_m, at which its frequency $\omega_0(T) \to 0$. This establishes Q_0 as the primary order parameter for the transformation.[14] The second term in Eq. (1) represents the energy necessary to produce a tetragonal strain u, and the third term represents the lowest-order nonvanishing coupling between Q_0 and u providing that Q_0 represents a phonon of symmetry type $\Gamma_{15}(+)$, $\Gamma_{15}(-)$, or $\Gamma_{25}(-)$ (see Table I). Because of this higher-order coupling, there is a resulting secondary tetragonal distortion of magnitude $u = (d/c)Q_0^2$, obtained by minimizing F_0 with respect to u.

Equation (1), however, is not of the proper functional form to discuss the sublattice distortions of $\Gamma_{12}(+)$ symmetry which are observed. It follows from the observation that the tetragonal strain components also transform as $\Gamma_{12}(+)$ that there exists a linear coupling between u and $\Gamma_{12}(+)$ optic-phonon displacements Q_1. Thus

$$F_1 = (\tfrac{1}{2}\omega_1^2 Q_1^2 + gQ_1 u + \tfrac{1}{2} cu^2) + \text{higher-order terms}. \quad (2)$$

In this case neither u nor Q_1 can be identified as the order parameter. The appropriate order parameter is rather a linear combination of tetragonal strain and sublattice distortion obtained by minimizing the quadratic terms in Eq. (2) with respect to Q_1.[15] A spontaneous strain thus automatically implies a *proportional* spontaneous sublattice displacement even in the absence of a "soft" optical frequency ω_1.[16] The sublattice displacements renormalize the stiffness against tetragonal strain to $c' = c - (g^2/\omega_1^2)$. One may then think of a lattice instability as arising from a softening of either $c(T)$ or $\omega_1(T)$, since both lead to $c'(T) \to 0$.[17] Theoretical considerations thus far have concentrated upon contributions of partially filled narrow electronic d bands to $c(T)$.[8-10]

Among the higher-order terms in Eq. (2) there are, in particular, the cubic terms u^3, u^2Q_1, etc., which cause the transformation to become discontinuous (first order), but this does not contradict most recent experimental findings.[12] Preliminary inelastic neutron scattering results have revealed interesting dynamical features associated with the phase transformation and more detailed studies are presently underway.

ACKNOWLEDGMENTS

We would like to thank B. W. Batterman, R. W. Cohen, J. J. Hanak, L. J. Vieland, and W. Rehwald for the loan of the excellent single crystal and for many stimulating discussions.

†Work performed under the auspices of the U.S. AEC.

[1]B. W. Batterman and C. B. Barrett, Phys. Rev. Letters 13, 390 (1964); Phys. Rev. 145, 296 (1966).

[2]K. R. Keller and J. J. Hanak, Phys. Rev. 154, 628 (1967); R. Rehwald, Phys. Letters 27A, 287 (1968).

[3]R. Mailfert, B. W. Batterman, and J. J. Hanah, Phys. Letters 24A, 315 (1967); Phys. Status Solidi 32, K67 (1969).

[4]For earlier references see, for example, a recent article by E. Pytte, Phys. Rev. (to be published).

[5]P. W. Anderson and E. J. Blount, Phys. Rev. Letters 14, 217 (1965).

[6]J. Perel, B. W. Batterman, and E. I. Blount, Phys. Rev. 166, 616 (1968).

[7]B. M. Klein and J. L. Birman, Phys. Rev. Letters 25, 1014 (1970).

[8]J. Labbé and J. Friedel, J. Phys. Radium 27, 153 (1966); 27, 303 (1966).

[9]G. D. Cody, R. W. Cohen, and L. J. Vieland, *Proceedings of the Eleventh International Conference on Low Temperature Physics*, edited by J. F. Allen *et al.* (St. Andrews U. P., St. Andrews, Scotland, 1969), p. 1009.

[10]E. Pytte, Phys. Rev. Letters 25, 1176 (1970).

[11]J. J. Hanak and H. S. Berman, *Crystal Growth* (Pergamon, New York, 1967), p. 249.

[12]L. J. Vieland, R. W. Cohen, and W. Rehwald, Phys. Rev. Letters 26, 373 (1971).

[13]G. Shirane and V. J. Minkiewicz, Nucl. Instr. Methods 89, 109 (1970).

[14]L. D. Landau and E. M. Lifshitz, *Statistical Physics* (Addison-Wesley, Reading, Mass., 1958), Chap. XIV.

[15]M. Born and K. Huang, *Dynamical Theory of Crystal*

Lattices (Clarendon, Oxford, England, 1954), p. 134ff.

[16]Had an optic mode of the type governed by Eq. (1) provided the primary instability, secondary distortions involving *both* tetragonal strains and $\Gamma_{12}(+)$ sublattice displacements would have resulted. However, inspection shows that arbitrary $\Gamma_{12}(+)$ displacements may be added to those listed in Table I without further lowering the symmetry of the space group.

[17]P. B. Miller and J. D. Axe, Phys. Rev. 163, 924 (1967).

PHYSICAL REVIEW B VOLUME 4, NUMBER 9 1 NOVEMBER 1971

Finite-Voltage Behavior of Lead-Copper-Lead Junctions*

John Clarke†

Department of Physics, University of California, Berkeley, California 94720
and Inorganic Materials Research Division, Lawrence Radiation Laboratory, Berkeley, California 94720

(Received 9 June 1971)

Pb-Cu-Pb junctions were made by evaporating successively on to a glass substrate a strip of Pb, a disk of Cu, and a second strip of Pb at right angles to the first. Each Pb strip had a width w. At liquid-He^4 temperatures, the junctions could sustain a dc Josephson supercurrent less than or equal to the critical current i_c. When i_c was small enough so that the Josephson penetration depth λ_J ($\propto i_c^{-1/2}$) was greater than $\frac{1}{4}w$, the supercurrent flowed uniformly through the junction, which was said to be "weak." When i_c was higher so that λ_J was less than $\frac{1}{4}w$, the supercurrents were nonuniform, and the junction was said to be "strong." At a current i greater than i_c, the voltage v across a weak junction was in reasonable agreement with the theoretical result $v=(i^2-i_c^2)^{1/2}R$, where R is the normal-state resistance of the Cu film. For strong junctions, a dc supercurrent appeared at finite voltages, because the ac supercurrents had a nonzero time average. The experimental results are in good qualitative agreement with calculations on a one-dimensional model. When the current was fed into the junction asymmetrically, that is, when it was applied to one end of each Pb strip, the self-field of the current generated periodic structure on the i-v characteristic, the period being typically 3 mA. The structure vanished if the currents were applied symmetrically, that is, the input and output currents divided equally between the ends of each lead strip. The application to a junction of rf electromagnetic radiation of angular frequency Ω induced constant-voltage current steps at voltages $(n/m)\hbar\Omega/(2e)$, where n and m are integers. The amplitude of the steps was modulated by the amplitude of the rf power and by a magnetic field in approximately the manner observed in tunnel junctions with oxide barriers. The dynamic resistance of the steps was less than $1.7\times10^{-14}\,\Omega$. The electrochemical potential across the junction at which a given step appeared was not affected by either junction material or experimental conditions at a precision of 1 part in 10^8. The highest frequency at which steps were induced was 2 MHz. At this frequency the skin depth of the copper was much less than w, and little radiation was coupled into the junction. The lowest frequency was 5 kHz, corresponding to a first-order induced step at about 10^{-11} V. At this voltage, the Johnson-noise broadening of the Josephson frequency was also about 5 kHz. At lower frequencies, the noise completely destroyed the synchronization between the Josephson ac supercurrents and the rf radiation, so that no steps were observed.

I. INTRODUCTION

An *SNS* junction consists of a thin film of a normal metal sandwiched between two superconductors. Each superconductor induces into the normal metal a finite pair amplitude[1-3] which decays exponentially[1-3] towards the middle of the normal layer. Provided the normal metal is not too thick, the overlap of the two pair wave functions will be large enough for the coupling energy[4,5] of the two superconductors to exceed the thermal fluctuation energy.[5-7] As a result, phase coherence will be established across the junction, and Josephson[5,7,8] tunneling becomes possible. It should be pointed out that the passage of a supercurrent through an *SNS* junction does in fact require a pair *tunneling* process. Although there are one-electron propagating states in the normal metal, the pairs induced in each side of the normal layer by the superconductors are in evanescent states,[2] and cannot support a supercurrent unless the two decaying wave functions overlap. Under these circumstances, the supercurrent i obeys the Josephson[6,9] current phase relation

$$i=i_c\sin\phi\,, \tag{1.1}$$

where i_c is the critical current (maximum supercurrent) and ϕ is the phase difference between the